Field emission from chemical vapor deposited diamond and diamond-like carbon films: Investigations of surface damage and conduction mechanisms

Paul W. May,[a] Stefan Höhn, and Michael N. R. Ashfold
School of Chemistry, University of Bristol, Bristol BS8 1TS, United Kingdom

Wang N. Wang, Neil A. Fox, Tim J. Davis, and J. W. Steeds
Department of Physics, University of Bristol, Tyndall Avenue, Bristol BS8 1TR, United Kingdom

(Received 16 February 1998; accepted 21 April 1998)

Field emission properties of undoped chemical vapor deposited diamond and diamond-like carbon films have been measured for a variety of different deposition conditions. The nature and appearance of the damage site after testing has been investigated with scanning electron microscopy and laser Raman mapping. These observations, together with the mathematical form of the observed current–voltage relations, are correlated with the conductivity of the film. The results are consistent with a model for the overall emission current that combines conduction mechanisms through the bulk of the film with Fowler–Nordheim tunneling. © *1998 American Institute of Physics.* [S0021-8979(98)01115-3]

I. INTRODUCTION

The emission of electrons from the surface of chemical vapor deposited (CVD) diamond and diamond-like carbon (DLC) films is currently of much interest due to potential applications in cold cathode devices. The negative electron affinity (NEA) of certain hydrogenated diamond surfaces plays an important role,[1] and the effect of different surface terminating species can greatly affect the emission characteristics.[2] However, since most of the results from low field emission experiments are from CVD diamond or DLC films with poorly characterized surfaces, it is clear that NEA is not solely responsible for the emission process. In fact, depending upon the construction of the electrical circuit, there are many different mechanisms involved as the electrons travel from the negative end of the power supply through the various interfacial contacts, through the bulk of the film itself, to the film surface, then tunnel through the potential barrier, propagate through the vacuum gap, before finally reaching the anode. The exact nature of the mechanisms occurring at each step in this process and the way in which they interact is still not well understood. The two basic models for carrier injection at a metal–insulator interface or a metal surface are Schottky emission and Fowler–Nordheim injection.[3] In both models, a potential barrier is created at the interface corresponding to the energy difference between the conduction band of the insulator and the Fermi level of the metal. In Schottky emission, carriers are injected over this barrier, whereas in the Fowler–Nordheim case, carriers tunnel through the barrier. In most current literature on field induced emission from diamond or DLC films, the current–voltage relation is simply fitted to a Fowler–Nordheim model, and a good fit has been taken as evidence that the process occurring is cold field emission. However, there are problems with the Fowler–Nordheim model when applied to diamond films. It was originally developed[4,5] as a model to explain emission from metals, and its application to materials with different band structures, such as semiconductors, is questionable. Further extending its application to wide band gap semiconductors or insulators, such as diamond, is therefore even more dubious. Other problems are that parameters extracted from the ''Fowler–Nordheim plot'' of $\ln(I/V^2)$ against $1/V$ (where I and V are the emission current and voltage, respectively) often have physically unrealistic values.[6] A question mark, therefore, hangs over the validity of using the Fowler–Nordheim model for diamond-based films, and also, therefore, over whether the dominant emission mechanism is really cold field emission at all.

In the bulk, conduction in undoped insulators is mainly controlled by deep levels in the band gap arising from defects or impurities. Whereas a conductor will obey Ohm's law (current is proportional to applied voltage), as the material becomes more insulating the charge can accumulate, restricting further increases in current as the voltage is increased. This is known as space charge limited current (SCLC),[7] and occurs in insulators at high applied field or high current densities. Poole–Frenkel (PF) conduction[8,9] is a different bulk process, which relies on there being a significant number of defect or impurity sites within the insulator. The charge carriers reside on these defect sites, and if the sites are sufficiently close together, the wave functions of the charge carriers may overlap, allowing the carriers to ''hop'' from one site to another. However, if the defects sites are too far apart, the hopping mechanism cannot keep up with the applied electric field, and the Poole–Frenkel current can become space-charge limited.[10] Conversely, for insulators with a high defect density, there can be an overlap of the Coulombic potentials of the defect sites, effectively lowering the barrier for carrier hopping. This gives rise to Hill type

[a]Electronic mail: paul.may@bris.ac.uk

conduction,[8] which can be thought of as a hopping process which includes nonlinearity at high fields.

Bulk conductivity experiments performed on undoped CVD diamond films[11–14] have shown that of the above models, the SCLC model can provide a good description of the dominant conduction mechanism. The magnitude of the space-charge currents in these experiments implied a band tail with a high density of states, increasing exponentially toward the valence band. The density of states measured in these experiments suggest that conduction occurs through highly disordered regions, such as might occur at the grain boundaries of polycrystalline films. As a result, grain boundaries have been proposed as the dominant conduction path through CVD diamond films.[15]

In this work we report the results of a series of field emission experiments performed upon undoped microcrystalline CVD diamond and amorphous DLC films produced using a variety of deposition conditions. By observing the morphology of the damaged area created by the field emission, and careful analysis of the mathematical form of the current–voltage dependence of the emission, insight into the conduction mechanisms in the various types of film can be obtained.

II. EXPERIMENT

The CVD diamond films were deposited onto Si(100) substrates (previously abraded with 1–3 μm diamond grit) using conditions typical for a hot filament CVD reactor[16] (process pressure 20 Torr, filament temperature 2300 °C, substrate temperature 900 °C, growth rate 0.5 μm h^{-1}). Films were grown for 6 h giving a film thickness of 3 μm. The process gas was a mixture of CH_4 in H_2, with three methane concentrations. 0.5% CH_4 produced high quality polycrystalline diamond films with crystallite size around 1 μm, 1% CH_4 produced good quality diamond with more grain boundaries and crystal size around 0.5μm, and 2% CH_4 produced poor quality ''ballas'' type diamond with crystal size around 0.05–0.1 μm.

The DLC films were deposited on mirror-polished (100) Si using a 13.56 MHz radio frequency parallel plate reactor and CH_4 as the sole process gas.[17] The process pressure was varied from 5 to 200 mTorr and the rf power from 10 to 300 W (dc self-bias 60–500 V) over an 8-cm-diam electrode. Deposition time was 30 min, producing smooth, featureless DLC films of 0.1–0.2 μm thickness. At powers greater than about 70 W, the films were hard, stressed and electrically insulating, with a higher degree of sp^3 character. With decreasing rf power, or increasing pressure, the films became softer and more graphitic, and were more electrically conducting.

The field emission characteristics of the films were tested using a diode configuration consisting of a cathode (the film under test) and a tungsten tip anode (cylinder shape, 0.5 mm diameter) mounted in a turbopumped vacuum chamber at a base pressure of 10^{-6} Torr. The tip-sample distance was con−tinuously adjustable to a few hundred μm. A negative voltage of up to 5 kV was applied to the cathode using a PC-controlled power supply, while the emission current was measured automatically as the voltage was ramped at a rate of $\sim$50 V s^{-1}. A current limit of 0.2 mA was set to avoid destruction of the films by excessive current flow. To minimize the effects of run-to-run inconsistencies, in each case current–voltage ($I-V$) data were measured for three films that had been deposited using identical conditions, and at two different places on each film. Values of the threshold voltage, and subsequent data analysis, were then calculated from an average of ten $I-V$ curves measured at each position on each sample — an average of 60 data sets in all.

During testing, it was found necessary to ramp the voltage up and down several times in order for the $I-V$ curves to stabilize and become reproducible. This conditioning or activation effect has been reported previously,[18] and is often accompanied by morphological changes on the film surface. For both CVD diamond and DLC films, the nature and appearance of the damaged site varies depending upon the properties of the film and the testing conditions. These damage sites are believed to occur as a result of extremely high local fields in the vicinity of the emission site causing dielectric breakdown of the surface, followed by rapid heating and vaporization of the surface layers.[19] Often the presence of such vapor phase species close to the surface, along with high fields, creates a plasma leading to a discharge, often observed as sparking between the electrodes.

The damage sites were studied using scanning electron microscopy (SEM) and laser Raman mapping (LRM). This latter technique was performed using a Renishaw Raman System 2000 incorporating an Ar ion laser operating at 488 nm. In LRM, Raman spectra are taken at a number of points in a line across the sample, with 25 μm resolution. This is repeated in two dimensions, and then followed by background subtraction and curve fitting of the data extracting only the wavelength regions of interest. The results are then displayed as two-dimensional intensity maps.

III. RESULTS AND DISCUSSION

A. The evolution of damage sites

Figure 1 shows the damage sites observed on a CVD diamond film after field emission testing for a variety of different emission currents and testing durations, with Fig. 1(a) showing the diamond surface before testing. The evolution of the damaged region can be seen as it undergoes several different morphological changes. The only visible sign of damage after extracting only a small current for a very short time is a blackening of the surface due to deposition of graphitic material [Fig. 1(b)]. With increased time/current [Fig. 1(c)], small indentations appear on the surface of the film. These indentations are similar in size to that of a single crystallite ($\sim$1 μm), and are less than 1 μm deep. Apart from the darkening of the surrounding area mentioned above, the crystals adjacent to these indentations appear unaffected. With further increases in current/time, the depressions deepen to form distinct craters which can go several μm into the film [Fig. 1(d)]. Some of these craters even extend down to the surface of the Si substrate, and when this happens some of the redeposited material is found to contain Si (see later). With still further increases in current or time, the num-

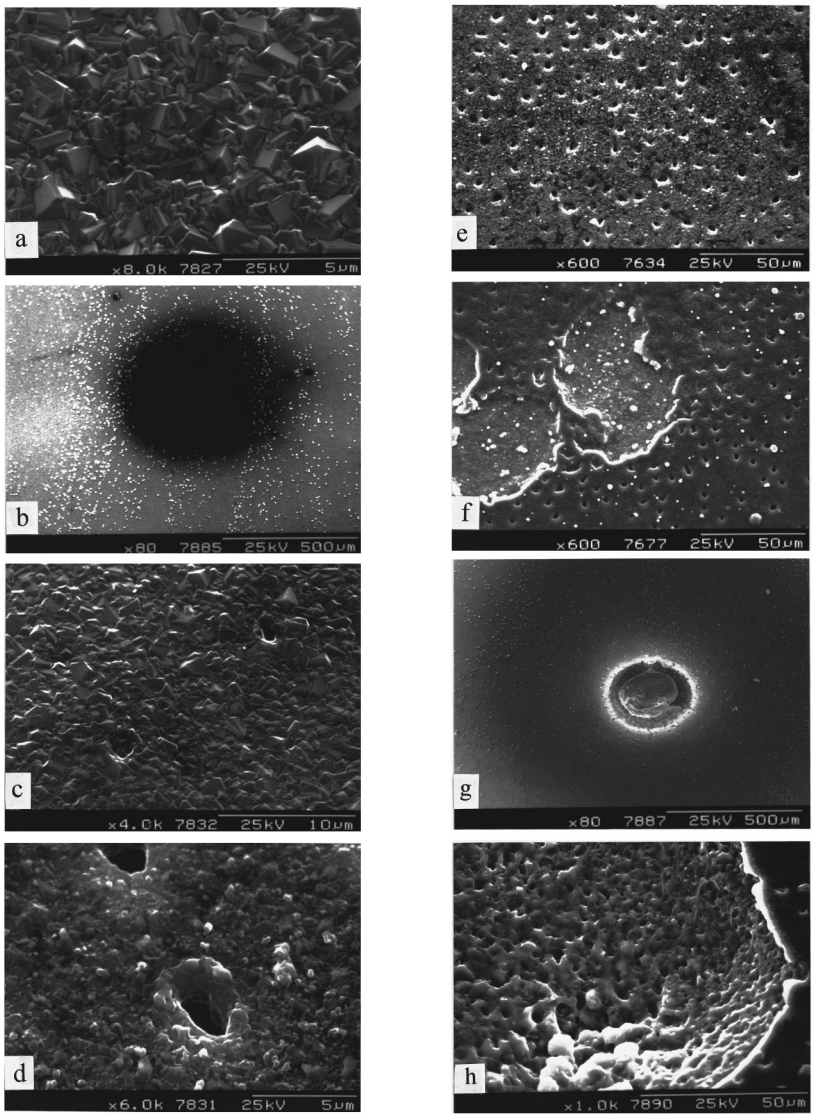

FIG. 1. Scanning electron micrographs of the damage sites observed after field emission testing on an undoped CVD diamond film grown with 1% CH_4 in H_2. (a) Before testing, a randomly oriented polycrystalline film with crystallite size around 1 μm, (b) after extracting a current of 1 μA for 60 s, the surface appears blackened but the crystal morphology is unchanged, (c) after 2 μA for 5 min, small depressions can now be seen on the surface of the film, going down to a depth of between 0.5 and 1 μm, (d) 2 μA for 30 min, individual craters now form, of diameter 1–5 μm and depth down to the surface of the Si substrate, the film in the vicinity of the craters appears rounded and partially melted, (e) 10 μA for 5 min, multiple even-spaced craters are now visible covering the entire 0.5 mm diameter tested area, (f) 10 μA for 30 min, the crater density has increased to the point at which some have joined, causing sections of the film to either delaminate or be burnt away, (g) 100 μA for 60 min, the entire tested area has been destroyed and the film completely removed, with (h) the Si substrate in the central area showing signs of melting and recrystallization.

ber and density of these craters increases. Figure 1(e) shows a portion of the tested area where multiple evenly spaced craters are visible. The remarkable uniformity of the crater distribution is probably a result of space-charge effects, where the charge density surrounding the electrons from an emission site prevents the emission of other electrons from other sites close by. Only at a sufficiently long distance away does the field decrease to a value where field emission is possible, and another crater can form. An alternative explanation could be that the presence of redeposited carbon and/or Si on the surface surrounding the crater may inhibit emission of electrons from nearby sites. As the current density increases still further, the distance between craters decreases, to the point where they begin to join together [Fig. 1(f)]. When this occurs, large patches of the surface are removed, either by the gradual erosion process thought to be responsible for cratering, or by delamination of parts of the film that have become isolated islands. With very high current densities, the film covering almost the entire tested area has been destroyed [Fig. 1(g)], and in the center of this damaged area the Si substrate appears melted and recrystallized [Fig. 1(h)].

B. Laser Raman Mapping

Figure 2 shows the results of laser Raman mapping of a damage crater produced after drawing a current of 100 μA for 10 min. The three maps (a)–(c) are displayed using suitable wavelength regions for diamond, graphite, and Si, respectively. In Figs. 2(a) and 2(b) the center of the crater

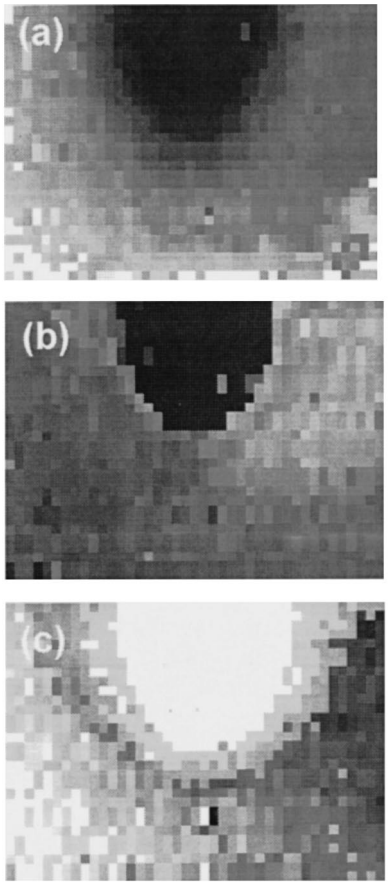

FIG. 2. Laser Raman intensity maps of a portion of a damage crater produced under conditions similar to those for Fig. 1(g), with a resolution of 25 μm. The size of the mapped area is 0.5 mm high by 1 mm across. The maps are viewed using selected Stokes shift wavelength regions for (a) diamond (1330–1340 cm^{-1}), (b) graphite (1450–1700 cm^{-1}) and (c) Si (510–530 cm^{-1}), with the grey-scale such that a white pixel corresponds to high signal intensity at that point.

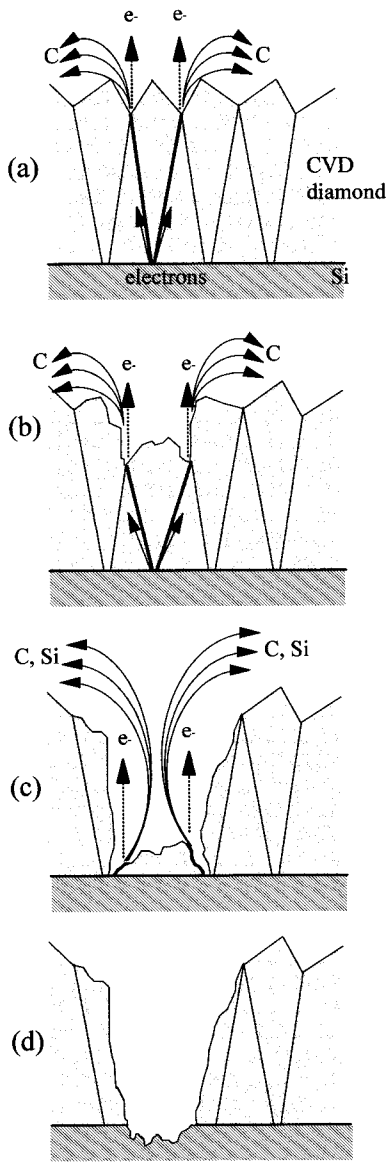

FIG. 3. Schematic diagram of crater formation and evolution during field emission testing from an undoped CVD diamond film. (a) Electrons originate from the interface between the diamond and the Si substrate, travel along the conductive graphitic pathways between the grains until they reach the surface where they undergo field emission into the vacuum. If the current density is sufficiently high, the conduction channels heat up and graphitization of the surrounding diamond begins to occur. Further sustained heating causes the carbonaceous material to evaporate or be sputtered from the surface, and then redeposited over the surrounding areas. (b) As graphitization and evaporation continue, a crater begins to form. Neighboring diamond crystallites are also partially graphitized by the local heating, and become rounded. (c) When the bottom of the crater comes sufficiently close to the Si substrate, this too begins to heat up, and Si is now evaporated and redeposited also. (d) When all the diamond has been destroyed, emission ceases from this site.

appears black, indicating the complete absence of diamond and graphite in this area. However, in Fig. 2(c) this area appears white due to the presence of Si. This shows that the film has been completely removed in this central region. Immediately surrounding the rim of the crater, we see enhanced signals for graphite and Si, possible resulting from the redeposition of evaporated material. Intensity due to graphite and Si can still be seen at distances greater than 0.25 mm from the edge of the crater, suggesting that these materials are ejected significant distances from the crater. At still further distances from the crater, the diamond signal begins to increase, suggesting that the thickness of the obscuring layer is decreasing.

C. Suggested mechanism for crater formation

Figure 3 shows a schematic diagram of the suggested mechanism for the formation of these damage craters in CVD diamond films. In Fig. 3(a) electrons originate from the interface between the diamond and the Si substrate.[20,21] They might then travel up the conductive pathways formed by the graphitic inclusions at the grain boundaries.[21] The columnar structure of a CVD diamond film, in which such conductive pathways are embedded in an insulating diamond matrix, can lead to a significant enhancement of the electric field. Lacher *et al.*[21] suggest that these graphitic inclusions may act as embedded field emission ''tips,'' facilitating the emission of electrons either directly into vacuum or into the conduction band of the surrounding diamond matrix. High current den-

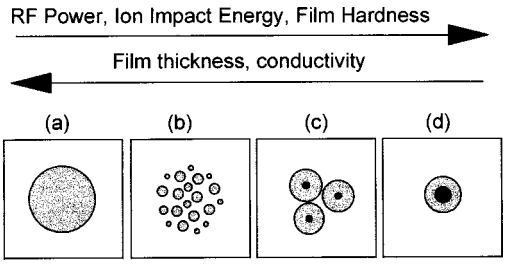

FIG. 4. Schematic diagram showing different types of damage site observed after field emission testing of DLC films grown using a range of rf powers. (a) <30 W, the DLC film has burnt off down to the Si substrate over a large area (0.5 mm diameter) corresponding to the size of the anode, (b) 30–70 W, many equally-spaced craters formed, (c) 80–100 W, only a few large craters, with the central section showing partial melting of the Si substrate, and (d) >100 W, a single large crater in the center of the tested area with extensive melting of the Si.

sities within the small volume of these conduction channels would lead to rapid local heating. It is feasible that local temperatures would easily exceed that required for graphitization of the surrounding diamond in vacuum ($\sim$1700 K).[22] This would increase the conductivity along these pathways resulting in, at first, a higher emission current. This has been suggested as one mechanism for the surface activation[23,24] mentioned earlier. The sputtering effect of the electric current (analogous to the electromigration effect seen in microprocessor interconnects), or simply the high temperatures, would cause the graphitic material to evaporate from the surface. With very high applied electric fields, this cloud of vapor phase species close to the surface may form a low resistance path for charge transport, resulting in a discharge between the electrodes and further damage to the diamond surface. With lower applied fields, however, it is likely that the evaporated material simply redeposits onto the surrounding surface.

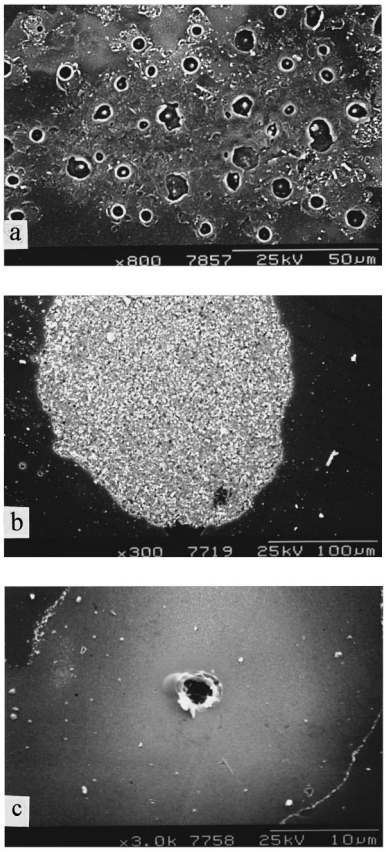

FIG. 5. Electron micrographs of the damage site from DLC films deposited at (a) medium power 50 W, (b) low power 20 W, and (c) high power 100 W, showing the cratering behavior illustrated schematically in Fig. 4.

TABLE I. The most usual mechanisms of conduction in insulators, their expected current voltage relations,[a] and mathematical relations required for a straight line plot.

Type of conduction	Current–voltage relation	Ordinate	Abscissa
Schottky emission	$I\sim\exp(aV^{1/2}/kT)$	$\ln I$	$\sqrt{V}$
Fowler–Nordheim	$I\sim V^2\exp(-a/V)$	$\ln(I/V^2)$	$1/V$
SCLC	$I\sim V$ (low fields)	I	V
	$I\sim V^n$ ($n>1$, high fields)	$\ln I$	$\ln V$
SCLC+PF	$I\sim V^2\exp(aV^{1/2}/kT)$	$\ln(I/V^2)$	$\sqrt{V}$
PF	$I\sim V\sinh(aV^{1/2}/kT)$	$\sinh^{-1}(I/V)$	$\sqrt{V}$
Hill's law	$I\sim\sinh(aV/kT)$	$\sinh^{-1} I$	V

[a]See Reference 14.

With increasing time or current, the depth of the crater increases, with more of the diamond being graphitized, evaporated, and redeposited [Fig. 3(b)]. At some stage, the depth of the crater is such that the surface of the Si substrate becomes exposed [Fig. 3(c)]. Since this, too, is subjected to the heating from the nearby conduction pathways, Si would now be ejected and redeposited along with carbon. Ultimately, after all of the diamond is destroyed, emission may cease at this site [Fig. 3(d)], whereupon nearby new surface sites may begin emitting instead.

D. Electron emission damage in DLC films

The same general mechanism may be true for DLC films, except that local heating may also cause a decrease in the hydrogen content of the film in the vicinity of the emission site — an effect which is also believed to enhance field emission.[24,25] The emission sites observed on DLC films are generally similar to those seen in CVD diamond films, except that for DLC we observed that the appearance of the damage site depended strongly upon the deposition conditions, along with the conductivity of the film (illustrated schematically in Fig. 4). Typically, a damage site appeared as in Fig. 5(a) for a DLC film deposited under medium power (say, 50 W) conditions. A number of equally-spaced craters are seen across the whole of the tested area (0.5 mm diameter). The similarity of these structures to the ones observed in CVD diamond [e.g., Fig. 1(d)–1(e)] suggests a common mechanism of formation in both types of films. It also implies that the structure of a DLC film may be described in a similar fashion to that of CVD diamond, i.e., conducting channels embedded in an insulating matrix. For DLC films produced at lower RF powers, i.e., softer, more conducting, graphitic films, the density of the craters increased, often linking up to form enlarged areas (tens or hundreds of μm across) where the film no longer existed and only the Si was visible [Fig. 5(b)]. In the case of DLC films deposited at powers less than $\sim$20 W, the crater density after

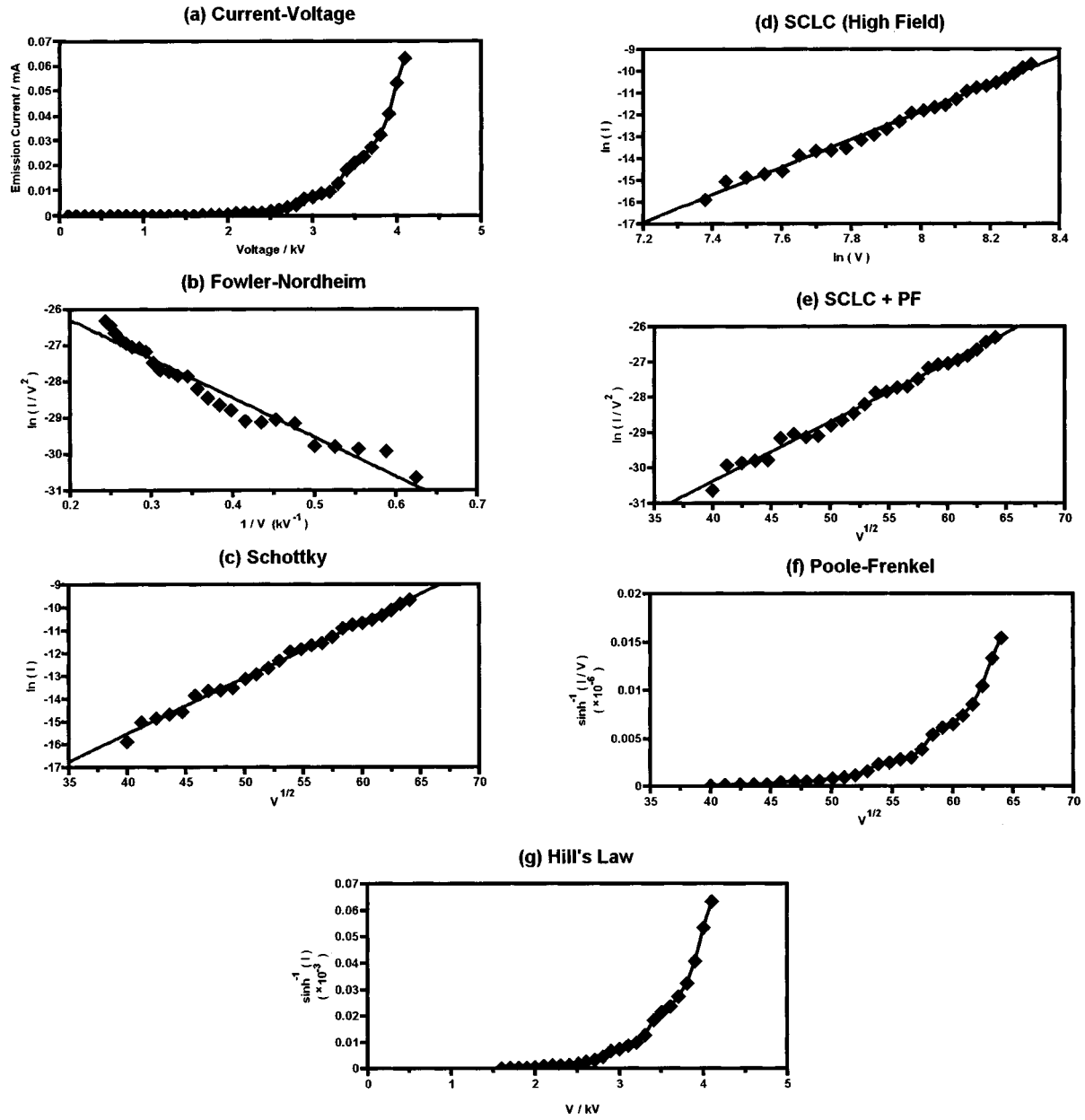

FIG. 6. Examples of plots from the various models for conduction in insulators. The data were taken from the emission results of a CVD diamond film grown with 0.5% CH_4 using a substrate-to-anode distance of 40 μm. The threshold voltage and the correlation coefficients for each model are given in Table II. In each graph, emission current (I) is measured in Amps and voltage (V) in V, unless stated otherwise. (a) A standard $I-V$ plot, (b) a Fowler–Nordheim plot showing only a reasonable fit to the data, (c) Schottky emission plot, showing a very good fit to the data, (d) SCLC high field plot [note that SCLC low field is identical to plot (a)] and (e) SCLC+PF, both showing very good fits to the data, (f) PF and (g) Hill's law plots, both showing nonlinear curves.

field emission testing was so large that the film over the entire 0.5-mm-diam tested area had been removed. Moreover, the exposed Si seemed much less damaged than for previous films, suggesting the DLC film had either delaminated or burnt off so rapidly that the local heating effect of the high current density had no chance to significantly affect the underlying Si. This could be because the current density had been shared between many neighboring emission sites, reducing the local current density below that needed to melt and vaporize Si. Conversely, for DLC films produced at high rf powers, the crater density decreased, ultimately to a single feature, located somewhere near the center of the tested area [Fig. 5(c)]. This shows the opposite extreme, in that the entire emission current was localized to only one site, causing excessive and very localized heating, producing either a large, deep crater (often down to a depth of several μm into the Si substrate), or sometimes a hillock of melted and recrystallized C and Si material. The amount of redeposited Si was significantly increased in these types of films also.

For CVD diamond films, this observed trend is generally similar, although not as pronounced. The ballas-type films grown with high methane concentration show damaged areas containing many linked craters, whereas the more crystalline, insulating films grown with low methane concentration, show fewer, isolated craters.

TABLE II. Threshold voltages (V_{th}) and correlation coefficients (r^2) for the straight lines of best fit for the different data plots given in Table I and various CVD diamond and DLC films. For the PF and Hill's Law plots, a straight line fit was inappropriate because the plot was obviously a curve, giving values of r^2 of <0.7 in each case. These have been omitted for brevity. To reduce scatter due to random error, the values for each film are averages from 60 sets of I–V data. Our estimated uncertainty in each of the quoted threshold voltages is ± 4 V, while the values for the correlation coefficients are reproducible to two decimal places.

	$V_{th}/V(\mu m^{-1})$	Fowler–Nordheim	Schottky	SCLC	SCLC+PF
CVD 0.5% CH_4	38	0.95	0.99	0.99	0.99
CVD 1% CH_4	25	0.96	0.99	0.98	0.98
CVD 3% CH_4	19	0.99	0.96	0.98	0.94
DLC 30 W	43	0.93	0.90	0.92	0.85
DLC 50 W	31	0.98	0.93	0.96	0.92
DLC 60 W	29	0.98	0.92	0.96	0.88
DLC 90 W	60	0.99	0.99	0.99	0.98

E. Field emission results

When discussing field emission, the most commonly used model for the ejection of electrons from a surface is the well-known Fowler–Nordheim equation.[3] However, this only deals with surface effects (or at the interface between the electrical contact and the film), and there are many other models for the mechanisms of conduction in the bulk of insulators[3] which may be important when studying field emission from diamond. The expected current–voltage relations for some of these models are given in Table I. By plotting the appropriate mathematical form of these relations as abscissa and ordinate, a straight line plot can be obtained. The correlation coefficient of the line of best fit then gives a direct measure of how well each model fits the experimental data. An example of each of these types of plots for one of the samples is given in Fig. 6, and Table II lists the results of such analyses for each of the CVD and DLC films investigated.

Beginning with the DLC films, we find that for the more conducting, softer DLC films, the Fowler–Nordheim model is a better fit than any of the other models [except for perhaps the space charge limited current (SCLC) model which is comparable]. However, as the films become harder and more insulating, some of these other models, in particular the Schottky emission, SCLC, and SCLC+Poole–Frenkel (SCLC+PF) models, provide increasingly better fits to the data, although the Fowler-Nordheim model is still the best. For very insulating films (e.g., the one grown at 90 W power), these other models provide as good a fit to the data as the Fowler–Nordheim model. In no cases did the standard PF or Hill's Law models produce a straight line, and so the mechanisms implied by these models can be ruled out as being significant in DLC films.

This trend is mirrored in the CVD diamond films, although the differences are not so clear cut: films grown under methane rich conditions are best modeled with the Fowler–Nordheim equation, whereas for the better quality films, other models perform as well, if not better. Indeed, for the high quality CVD film grown using 0.5% CH_4, the Schottky emission, high field SCLC and SCLC+PF models appear to provide much better descriptions of the overall conduction mechanism than the Fowler–Nordheim model.

A possible explanation for these observations can be made using arguments similar to those stated above. For conducting films, the significant mechanism is probably only the tunnelling of the electrons through the potential barrier, since conduction through the film would be relatively facile. For more insulating films, however, conduction through the bulk of the film might become important and potentially rate limiting. Thus, bulk conduction mechanisms (such as SCLC), as well as mechanisms occurring at the various interfaces (such as Schottky emission), may begin to play a significant role in the electron transport. If this is true, the observed current–voltage dependence will be a combination of these mechanisms and the Fowler–Nordheim surface ejection model.

An alternative mechanism, however, might involve the Si which is often evaporated from the bottom of the craters to redeposit onto the film surface. The presence of a thin Si layer covering the area immediately surrounding an emission site may affect the local emission characteristics in an unknown way. It is already known[2] that the presence of different terminating species on a diamond surface, and/or thin layers of electropositive metals, such as Na or Cs, greatly affect the observed emission characteristics. Since we observed a greater tendency for Si evaporation on the less conductive diamond-like films, it is possible that the presence of this Si coating might be responsible for the non-Fowler–Nordheim contribution to the overall emission characteristics.

In conclusion, the observations presented in this article have given an insight into the conduction processes occurring in *undoped* CVD diamond and DLC films, as well as mechanisms by which emission causes the breakdown and destruction of the film. This may have implications for the lifetime of field emission devices. For the more insulating diamond and DLC films, electrical conduction through the film bulk is a process which should not be overlooked, since it contributes to the overall observed emission characteristics. A more general conclusion from this work, however, is that a straight line obtained in a Fowler–Nordheim plot of $I-V$ data obtained from diamond or DLC films does not necessarily prove that the electron emission process is cold field emission. Indeed, with four different mechanisms based on entirely different models for the carrier transport mecha-

nism, all giving good fits to the emission data, it is not obvious why one model should be used in preference to any other. Clearly, in future, if the Fowler–Nordheim model is to be used in preference to any other model, authors will need to justify their decision carefully. This will be especially important if reliable (and physically realistic) values for the emission area, surface work function and field enhancement factor, are extracted from the gradient and intercept of the plot.

This work has been concerned only with undoped films, and the relevance of this to the more highly doped, and therefore more conducting films, which are likely to be used when fabricating real devices, is still unclear. More work needs to be done, therefore, to study the effects of diamond doping level upon field emission and crater formation. The effect of substrate conductivity is also an area which needs attention.

ACKNOWLEDGMENTS

One of the authors (P.W.M.) wishes to thank the Royal Society for financial support and the award of a University Research Fellowship. The author (S.H.) also thanks the Socrates & Youth Technical Assistance Office of the EU for financial help.

[1] C. Bandis and B. B. Pate, Appl. Phys. Lett. **69**, 366 (1996).
[2] P. W. May, J. C. Stone, M. N. R. Ashfold, K. R. Hallam, W. N. Wang, and N. A. Fox, Diamond Relat. Mater. **7**, 671 (1998).
[3] J. J. O'Dwyer, *The Theory of Electrical Conduction and Breakdown in Solid Dielectrics* (Clarendon, Oxford, 1973).
[4] R. H. Fowler and L. Nordheim, Proc. R. Soc. London **A199**, 173 (1928).
[5] R. F. Burgess, H. Kroemer, and J. M. Houston, Phys. Rev. **90**, 515 (1953).
[6] S. R. P. Silva and R. G. Forbes, Ultramicroscopy (in press).
[7] M. A. Lampert and P. Mark, *Current Injection in Solids* (Academic, New York, 1970).
[8] R. M. Hill, Philos. Mag. **23**, 59 (1971).
[9] Y. Muto, T. Sugino, J. Shirafuji, and K. Kobashi, Appl. Phys. Lett. **59**, 843 (1991).
[10] P. N. Murgatroyd, J. Phys. D: Appl. Phys. **3**, 151 (1970).
[11] S. Ashok, K. Srikanth, A. Badzian, T. Badzian, and R. Messier, Appl. Phys. Lett. **50**, 763 (1987).
[12] J. Mort, M. A. Maconkin, and K. Okumura, Appl. Phys. Lett. **59**, 455 (1991).
[13] M. Werner, O. Dorsch, A. Hinze, E. Obermeier, R. E. Harper, C. Johnston, P. R. Chalker, and I. M. Buckley-Golder, Diamond Relat. Mater. **2**, 825 (1993).
[14] P. Gonon, A. Deneuville, F. Fontaine, and E. Gheeraert, J. Appl. Phys. **78**, 6633 (1995), and references therein.
[15] B. Fiegl, R. Kuhnert, M. Ben-Chorin, and F. Koch, Appl. Phys. Lett. **65**, 371 (1994).
[16] C. A. Rego, R. S. Tsang, P. W. May, M. N. R. Ashfold, and K. N. Rosser, J. Appl. Phys. **79**, 7264 (1996).
[17] M -T. Kuo, P. W. May, and M. N. R. Ashfold, Diamond Relat. Mater. (in press); S. Fletcher, BSc thesis, School of Chemistry, University of Bristol, UK, 1997.
[18] N. A. Fox, W. N. Wang, T. J. Davis, J. W. Steeds, and P. W. May, Appl. Phys. Lett. **71**, 2337 (1997).
[19] R. Hessmer, M. Schreck, S. Geier, and B. Stritzker, Diamond Relat. Mater. **3**, 951 (1994).
[20] W. Zhu, G. P. Kochanski, and S. Jin, Mater. Res. Soc. Symp. Proc. **416**, 443 (1996).
[21] F. Lacher, C. Wild, D. Behr, and P. Koidl, Diamond Relat. Mater. **6**, 1111 (1997).
[22] J. Wilks and E. Wilks, *Properties and Applications of Diamond* (Butterworth Heinemann, Oxford, 1991).
[23] R. Wächter, A. Cordery, S. Proffitt, and J. S. Foord, Diamond Relat. Mater. **7**, 687 (1998).
[24] O. Gröning, O. M. Kuttel, P. Gröning, and L. Slapbach, Appl. Surf. Sci. **111**, 135 (1997).
[25] K. C. Park, J. H. Moon, S. J. Chung, M. H. Oh, W. I. Milne, and J. Jang, J. Vac. Sci. Technol. B **15**, 428 (1997).